Antisymmetric Seebeck Effect in a Tilted Weyl Semimetal

Bingyan Jiang,[1] Jiaji Zhao,[1] Jiangyuan Qian,[2,3] Shen Zhang,[4] XiaoBin Qiang,[2,3] Lujunyu Wang,[1] Ran Bi,[1] Juewen Fan,[1] Hai-Zhou Lu,[2,3,*] Enke Liu,[4,5,†] and Xiaosong Wu[1,6,7,‡]

[1]*State Key Laboratory for Artificial Microstructure and Mesoscopic Physics, Frontiers Science Center for Nano-optoelectronics, Peking University, Beijing 100871, China*

[2]*Shenzhen Institute for Quantum Science and Engineering and Department of Physics, Southern University of Science and Technology (SUSTech), Shenzhen 518055, China*

[3]*Shenzhen Key Laboratory of Quantum Science and Engineering, Shenzhen 518055, China*

[4]*Beijing National Laboratory for Condensed Matter Physics, Institute of Physics, Chinese Academy of Sciences, Beijing 100190, China*

[5]*Songshan Lake Materials Laboratory, Dongguan 523808, China*

[6]*Collaborative Innovation Center of Quantum Matter, Beijing 100871, China*

[7]*Peking University Yangtze Delta Institute of Optoelectronics, Nantong 226010, Jiangsu, China*

Abstract

Tilting the Weyl cone breaks the Lorentz invariance and enriches the Weyl physics. Here, we report the observation of a magnetic-field-antisymmetric Seebeck effect in a tilted Weyl semimetal, $Co_3Sn_2S_2$. Moreover, it is found that the Seebeck effect and the Nernst effect are antisymmetric in both the in-plane magnetic field and the magnetization. We attribute these exotic effects to the one-dimensional chiral anomaly and phase space correction due to the Berry curvature. The observation is further reproduced by a theoretical calculation, taking into account the orbital magnetization.

Weyl Semimetals resources

- Book by Andrei Berneivig: Topological insulator, Springer 2015
- Lecture of Andrei Berneivig on Dirac and Weyl Semimetals at summer school TSM16 (available on youtube)
- Contact me on kesharpu@theor.jinr.ru, for tons of other resources on this subject

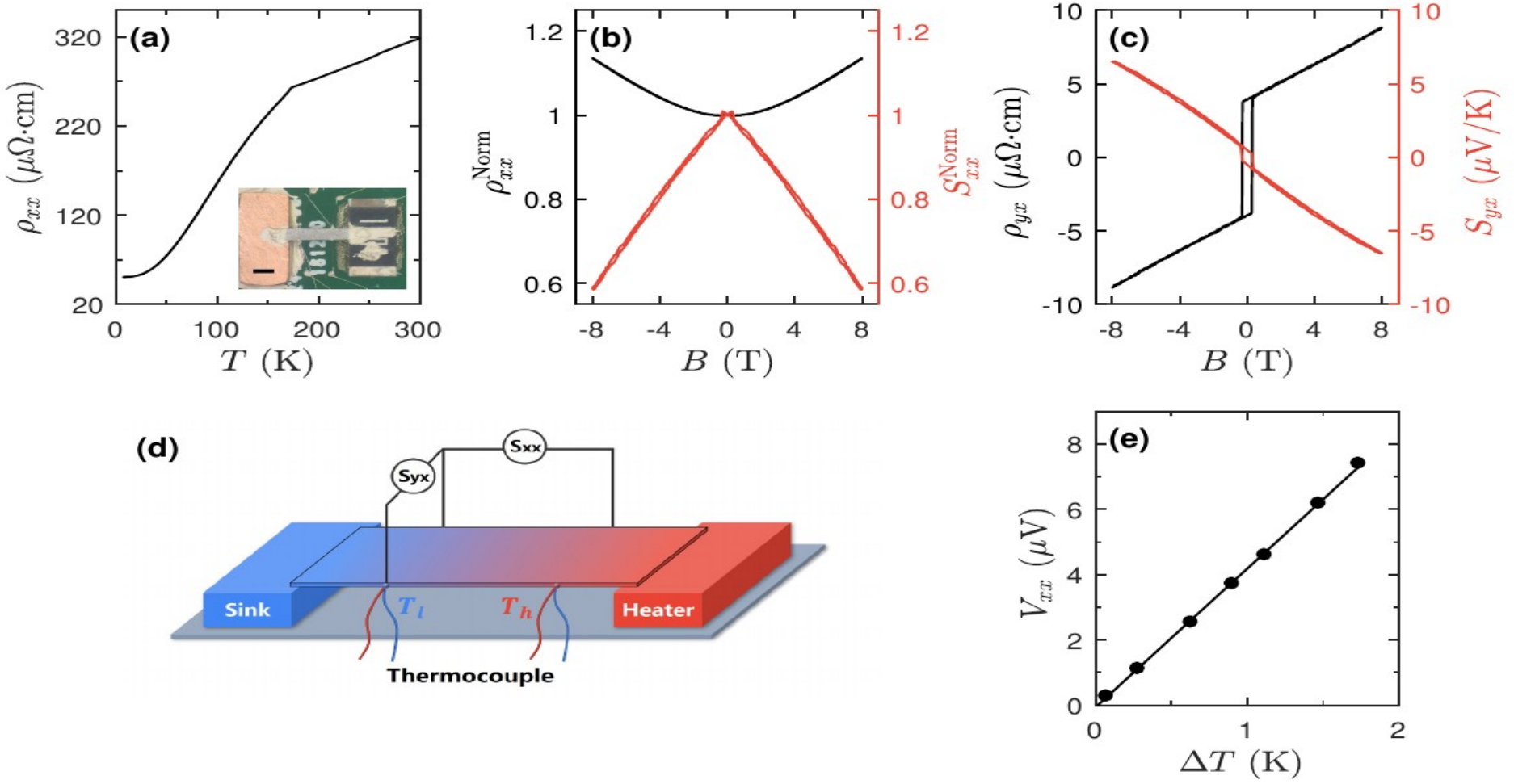
(a)
320
220
120
20
0
100
200
300
T (K)
ρ_{xx} ($\mu\Omega$·cm)
(b)
1.2
1
0.8
0.6
-8
-4
0
4
8
B (T)
$\rho_{xx}^{\mathrm{Norm}}$
S_{xx}^{Norm}
(c)
10
5
0
-5
-10
B (T)
ρ_{yx} ($\mu\Omega$·cm)
S_{yx} (μV/K)
(d)
Sxx
Syx
Sink
Heater
T_l
T_h
Thermocouple
(e)
8
6
4
2
0
1
2
ΔT (K)
V_{xx} (μV)

FIG. 1. Basic transport properties of $Co_3Sn_2S_2$ crystal and thermoelectric measurement setup. (a) Temperature dependence of longitudinal resistivity. A kink is observed at the Curie temperature $T_c = 175$ K. The inset is an optical image of the thermoelectric measurement setup. The scale bar is 1 mm. (b) Normalized longitudinal resistivity ρ_{xx} (black) and Seebeck coefficient S_{xx} (red) as a function of the perpendicular magnetic field at $T = 20$ K. The positive parabolic MR implies a dominant classic mechanism, while a negative and almost linear Seebeck may be attributed to the magnon-drag effect. (c) Anomalous Hall effect (black) and anomalous Nernst effect (red) at $T = 20$ K. (d) Diagram of thermoelectric measurement setup. Two thermocouples are attached at the edge of the sample. (e) Longitudinal thermoelectric signal V_{xx} as a function of the temperature difference ΔT. A linear dependence verifies the validation of our thermoelectric measurements.

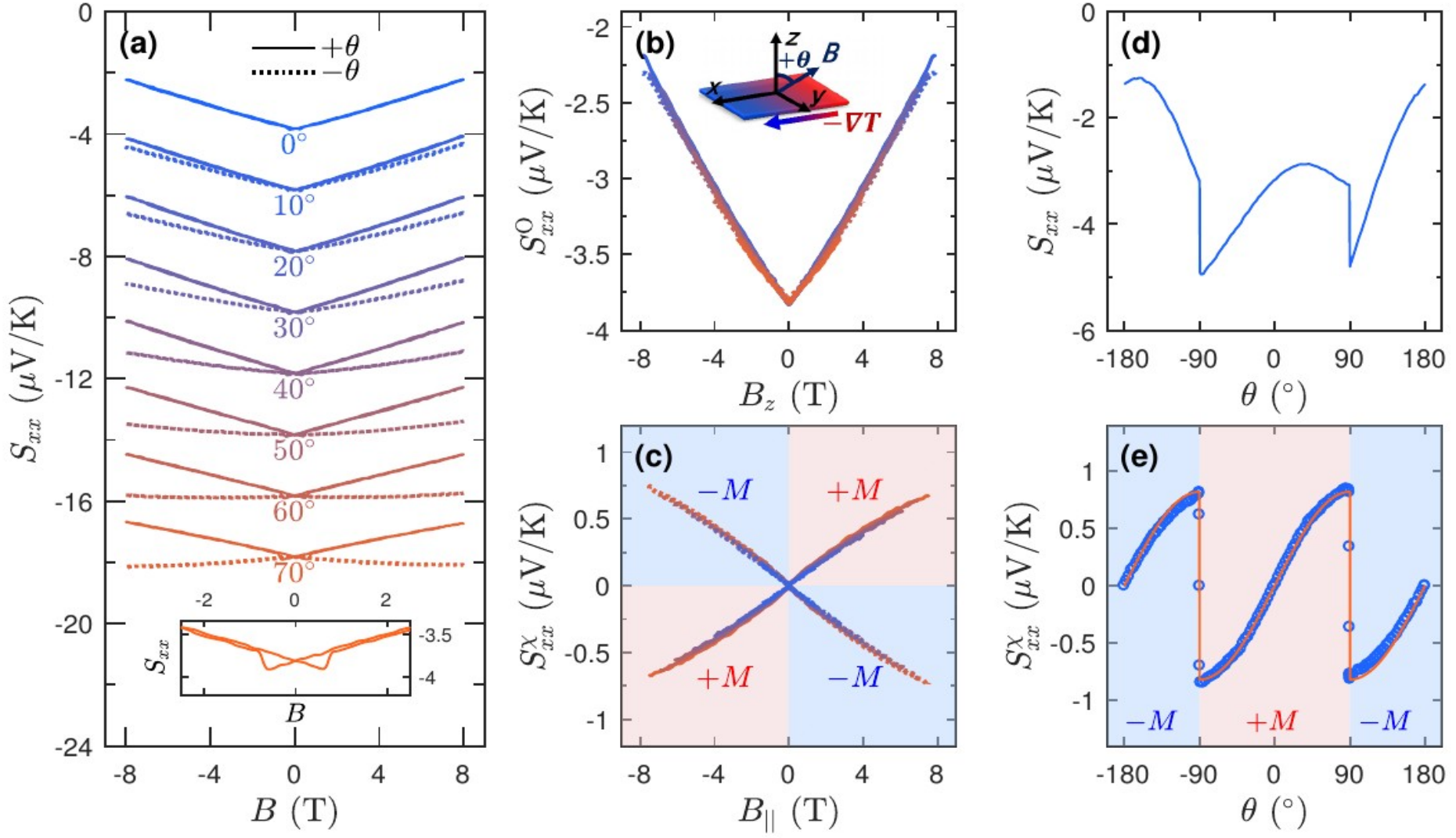
(a)
+θ
−θ
0°
10°
20°
30°
40°
50°
60°
70°
S_{xx} (μV/K)
B (T)
(b)
z
+θ
B
x
y
−∇T
S^O_{xx} (μV/K)
B_z (T)
(c)
−M
+M
+M
−M
S^χ_{xx} (μV/K)
$B_{||}$ (T)
(d)
S_{xx} (μV/K)
θ (°)
(e)
−M
+M
−M
S^χ_{xx} (μV/K)
θ (°)

FIG. 2. B- and M-antisymmetric Seebeck coefficient when $\mathbf{B} \perp \hat{x}$. (a) S_{xx} as a function of the magnetic field at different angles. Data are shifted for clarity. Traces at $\pm\theta$ diverge with increasing field and angle. The inset shows the field dependence of S_{xx} at $\theta = 70°$ at the low field region. Below B_c, the slope of the linear dependence shows opposite sign for $\pm M$. (b) S_{xx}^{O} as a function of B_z at different angles. The inset depicts the measurement setup and the angle definition. (c) S_{xx}^{χ} as a function of $B_{\parallel}$. For positive (solid line) and negative (dashed line) magnetization, the slopes display opposite signs. (d) Angular dependence of S_{xx} at $B = 8$ T. There exists a pronounced asymmetry with respect to $\theta = 0$. Because of the contact misalignment, there is a component of S_{yx}. Since S_{yx} is nearly symmetric in θ when $B \perp x$, as seen in Fig. S7, it does not affect the extracted S_{xx}^{χ}. It is evident that S_{xx}^{χ} in (e) is very close to that in Fig. S7(e)[47], which is extracted after removing the S_{yx}. (e) S_{xx}^{χ} versus θ. S_{xx}^{χ} is obtained by θ antisymmetrizing the data in (d). Open circles are experimental data and the solid lines are best fits to $\sin\theta$.

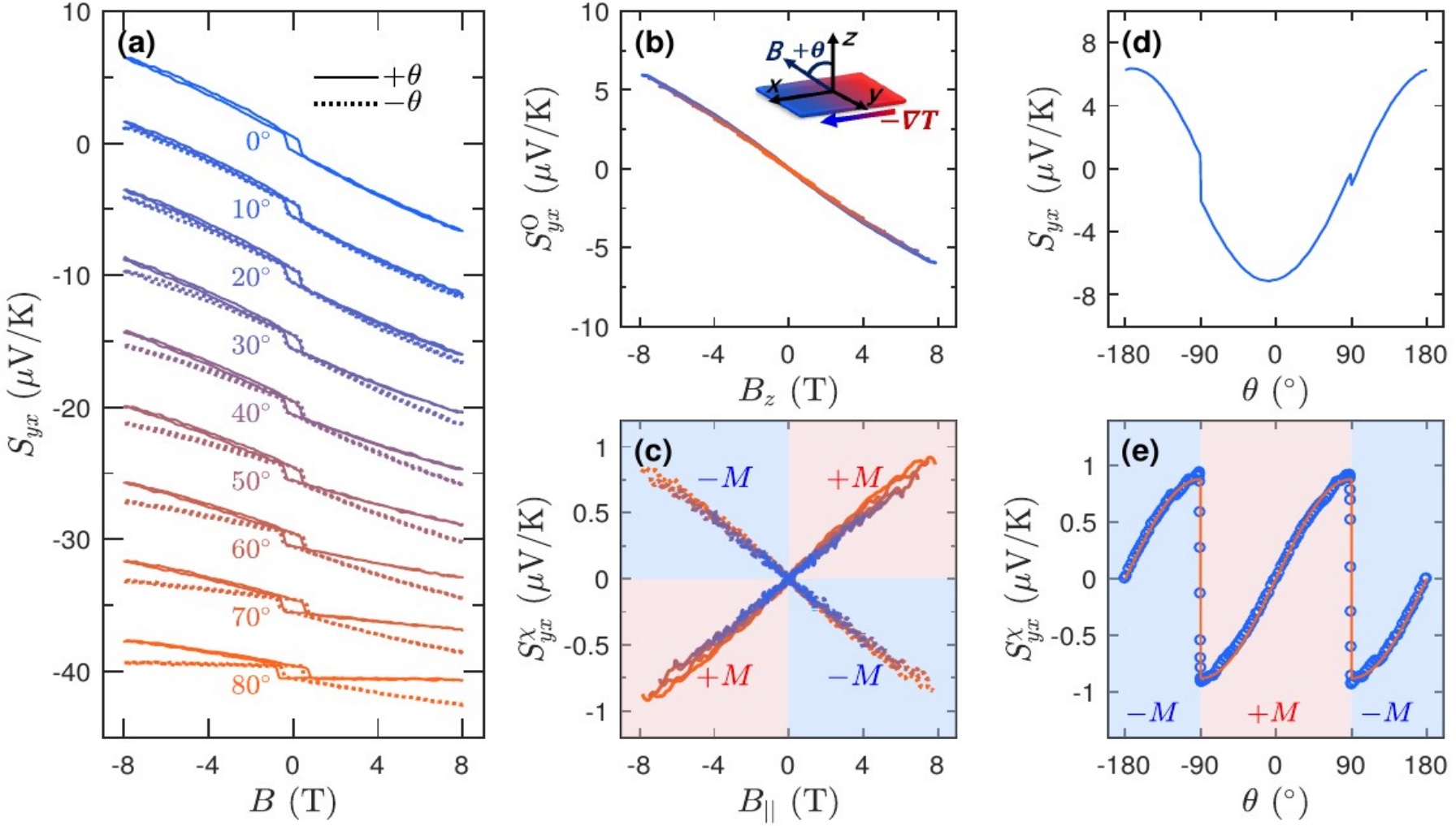
(a)
+θ
−θ
0°
10°
20°
30°
40°
50°
60°
70°
80°
S_{yx} (μV/K)
B (T)
(b)
B +θ
z
x
y
−∇T
S^{O}_{yx} (μV/K)
B_z (T)
(c)
−M
+M
+M
−M
S^{χ}_{yx} (μV/K)
$B_{||}$ (T)
(d)
S_{yx} (μV/K)
θ (°)
(e)
−M
+M
−M
S^{χ}_{yx} (μV/K)
θ (°)

FIG. 3. B- and M-antisymmetric Nernst effect when $\mathbf{B} \perp \hat{y}$. (a) Field dependence of Nernst signals at different angles. Data are shifted for clarity. Traces at $\pm\theta$ diverge with increasing field and angle. (b) S_{yx}^{O} versus B_z at different angles. The inset depicts the rotation angle. (c) S_{yx}^{χ} versus $B_{\parallel}$. The slope of the field dependence changes sign with M. (d) Angular dependence of S_{yx} at $B = 8$ T. There exists a pronounced asymmetry with respect to $\theta = 0$. Because of the contact misalignment, there is a slight component of S_{xx}. Moreover, it is nearly symmetric in θ when $B \perp y$, as seen in Fig. S6 [47]. Therefore, it does not affect the extracted S_{yx}^{χ}. (e) S_{yx}^{χ} versus θ. S_{yx}^{χ} is obtained by θ antisymmetrizing the data in (d). Open circles are experimental data and the solid lines are best fits to $\sin\theta$.